THE JOURNAL OF BIOLOGICAL CHEMISTRY VOL. 284, NO. 25, pp. 17129–17137, June 19, 2009

Defining the Structural Basis of Human Plasminogen Binding by Streptococcal Surface Enolase*[S][◆]

Received for publication, February 27, 2009, and in revised form, April 5, 2009 Published, JBC Papers in Press, April 10, 2009, DOI 10.1074/jbc.M109.004317

Amanda J. Cork[‡1], Slobodan Jergic[§], Sven Hammerschmidt[¶], Bostjan Kobe[‖2], Vijay Pancholi[**], Justin L. P. Benesch[‡‡3], Carol V. Robinson[‡‡4], Nicholas E. Dixon[§5], J. Andrew Aquilina[‡6], and Mark J. Walker[‡7]

From the [‡]School of Biological Sciences and [§]School of Chemistry, University of Wollongong, Wollongong NSW 2522, Australia, the [¶]Department of Genetics of Microorganisms, Institute for Genetics and Functional Genomics, Ernst-Moritz-Arndt University of Greifswald, Greifswald D-17487, Germany, the [‖]School of Molecular and Microbial Sciences and Institute for Molecular Bioscience, University of Queensland, Brisbane QLD 4072, Australia, the [**]Department of Pathology, Ohio State University, Columbus, Ohio 43210, and the [‡‡]Department of Chemistry, University of Cambridge, Cambridge CB2 1TN, United Kingdom

The flesh-eating bacterium group A *Streptococcus* (GAS) binds and activates human plasminogen, promoting invasive disease. Streptococcal surface enolase (SEN), a glycolytic pathway enzyme, is an identified plasminogen receptor of GAS. Here we used mass spectrometry (MS) to confirm that GAS SEN is octameric, thereby validating *in silico* modeling based on the crystal structure of *Streptococcus pneumoniae* α-enolase. Site-directed mutagenesis of surface-located lysine residues ($SEN^{K252+255A}$, SEN^{K304A}, SEN^{K334A}, SEN^{K344E}, SEN^{K435L}, and $SEN^{\Delta 434-435}$) was used to examine their roles in maintaining structural integrity, enzymatic function, and plasminogen binding. Structural integrity of the GAS SEN octamer was retained for all mutants except SEN^{K344E}, as determined by circular dichroism spectroscopy and MS. However, ion mobility MS revealed distinct differences in the stability of several mutant octamers in comparison with wild type. Enzymatic analysis indicated that SEN^{K344E} had lost α-enolase activity, which was also reduced in SEN^{K334A} and $SEN^{\Delta 434-435}$. Surface plasmon resonance demonstrated that the capacity to bind human plasminogen was abolished in $SEN^{K252+255A}$, SEN^{K435L}, and $SEN^{\Delta 434-435}$. The lysine residues at positions 252, 255, 434, and 435 therefore play a concerted role in plasminogen acquisition. This study demonstrates the ability of combining *in silico* structural modeling with ion mobility-MS validation for undertaking functional studies on complex protein structures.

Streptococcus pyogenes (group A *Streptococcus*, GAS)[8] is a common bacterial pathogen, causing over 700 million human disease episodes each year (1). These range from serious life-threatening invasive diseases including necrotizing fasciitis and streptococcal toxic shock-like syndrome to non-invasive infections like pharyngitis and pyoderma. Invasive disease, in combination with postinfection immune sequelae including rheumatic heart disease and acute poststreptococcal glomerulonephritis, account for over half a million deaths each year (1). Although a resurgence of GAS invasive infections has occurred in western countries since the mid-1980s, disease burden is much greater in developing countries and indigenous populations of developed nations, where GAS infections are endemic (2–4).

GAS is able to bind human plasminogen and activate the captured zymogen to the serine protease plasmin (5–17). The capacity of GAS to do this plays a critical role in virulence and invasive disease initiation (3, 17–19). The plasminogen activation system in humans is an important and highly regulated process that is responsible for breakdown of extracellular matrix components, dissolution of blood clots, and cell migration (20, 21). Plasminogen is a 92-kDa zymogen that circulates in human plasma at a concentration of 2 μM (22). It consists of a binding region of five homologous triple loop kringle domains and an N-terminal serine protease domain that flank the Arg^{561}–Val^{562} site (23), where it is cleaved by tissue plasminogen activator and urokinase plasminogen activator to yield the active protease plasmin (20, 23). GAS also has the ability to activate human plasminogen by secreting the virulence determinant streptokinase. Streptokinase forms stable complexes with plasminogen or plasmin, both of which exhibit plasmin activity (20, 24). Activation of plasminogen by the plasmin-(ogen)-streptokinase complex circumvents regulation by the host plasminogen activation inhibitors, α_2-antiplasmin and α_2-macroglobulin (11, 20). GAS can bind the plasmin(ogen)-streptokinase complex and/or plasmin(ogen) directly via plasmin(ogen) receptors at the bacterial cell surface (6). These receptors include the plasminogen-binding group A streptococcal M-like protein (PAM) (25), the PAM-related protein (19), glyceraldehyde-3-phosphate dehydrogenase (GAPDH; also known as streptococcal plasmin receptor, Plr, or streptococcal surface dehydrogenase) (9, 26), and streptococcal surface enolase (SEN or α-enolase) (27). Interactions with these GAS receptors occurs via lysine-binding sites within the kringle domains of plasminogen (6).

* This work was supported by the National Health and Medical Research Council (NHMRC) of Australia Grant 459103.
◆ This article was selected as a Paper of the Week.
[S] The on-line version of this article (available at http://www.jbc.org) contains a supplemental table and two supplemental figures.
[1] A recipient of a University of Wollongong Postgraduate Award.
[2] An Australian Research Council (ARC) Federation Fellow and an NHMRC Honorary Research Fellow.
[3] A Royal Society University Research Fellow.
[4] A Royal Society Professor.
[5] An ARC Australian Professorial Fellow.
[6] An NHMRC R. D. Wright Fellow.
[7] To whom correspondence should be addressed: School of Biological Sciences, University of Wollongong, Northfields Ave., Wollongong NSW 2522, Australia. Tel.: 61-2-4221-3439; Fax: 61-2-4221-4135; E-mail: mwalker@uow.edu.au.
[8] The abbreviations used are: GAS, group A *Streptococcus*; SEN, surface enolase; MS, mass spectrometry; IM, ion mobility; ESI, electrospray mass ionization; Tof, time-of-flight; mbar, millibar.

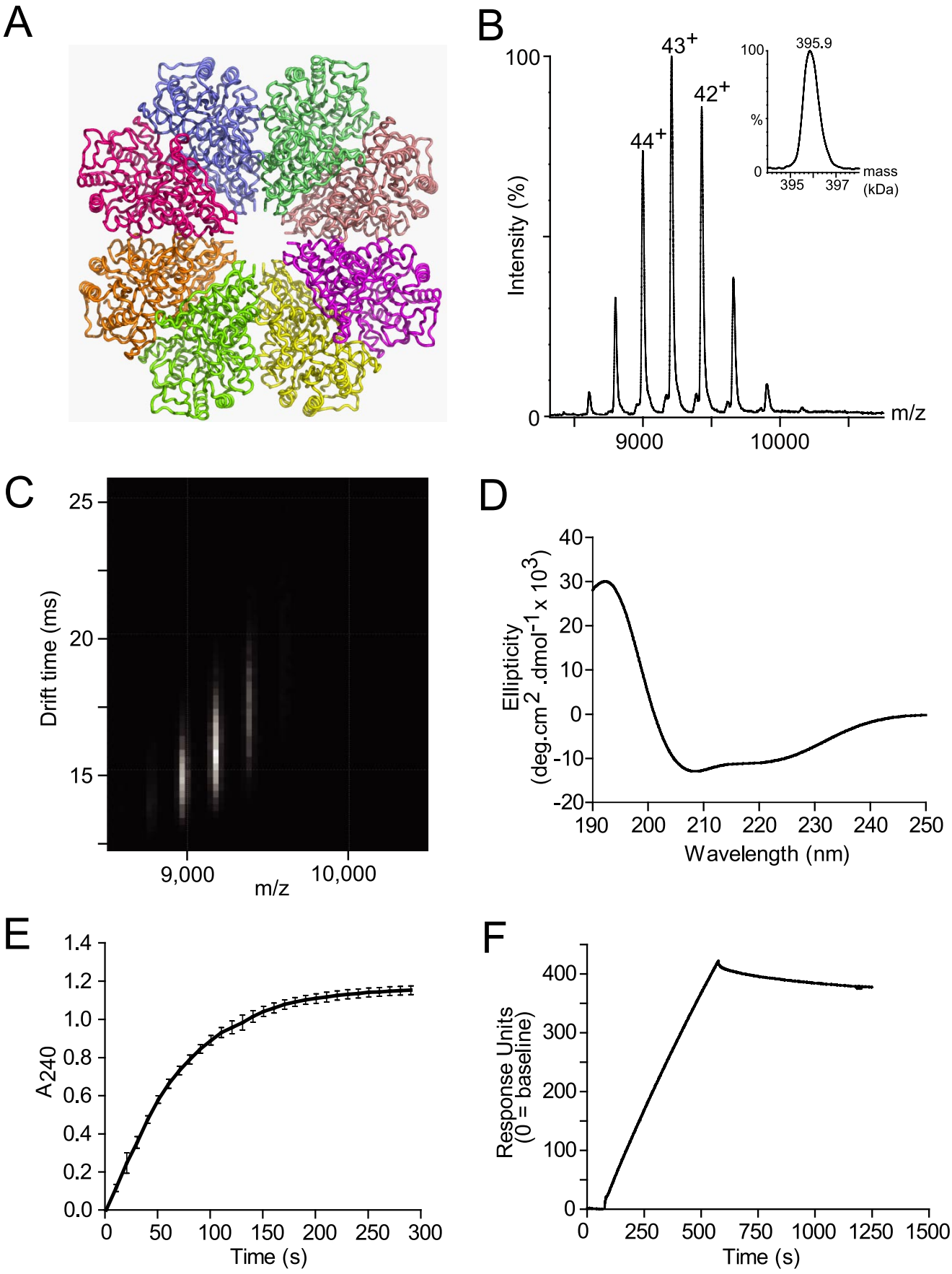
A
B
100
Intensity (%)
0
9000
10000
m/z
43+
42+
44+
100
395.9
%
0
395
397
mass
(kDa)
C
25
20
15
Drift time (ms)
9,000
10,000
m/z
D
40
30
20
10
0
-10
-20
Ellipticity
(deg.cm2.dmol-1 x 103)
190
200
210
220
230
240
250
Wavelength (nm)
E
1.4
1.2
1.0
0.8
0.6
0.4
0.2
0.0
A240
0
50
100
150
200
250
300
Time (s)
F
400
300
200
100
0
Response Units
(0 = baseline)
0
250
500
750
1000
1250
1500
Time (s)

In addition to its ability to bind human plasminogen, SEN is primarily the glycolytic enzyme that converts 2-phosphoglycerate to phosphoenolpyruvate (27–29). SEN is abundantly expressed in the cytosol of most bacterial species but has also been identified as a surface-located protein in GAS and other bacteria including pneumococci, despite lacking classical cell surface protein motifs such as a signal sequence, membrane-spanning domain, or cell-wall anchor motif (27, 28, 30, 31). The interaction between SEN and plasminogen is reported to be facilitated by the two C-terminal lysine residues at positions 434 and 435 (27, 32). In contrast, an internal binding motif containing lysines at positions 252 and 255 in the closely related α-enolase of *Streptococcus pneumoniae* has been shown to play a pivotal role in the acquisition of plasminogen in this bacterial species (33). The octameric pneumococcal α-enolase structure consists of a tetramer of dimers. Hence, potential binding sites could be buried in the interface between subunits. In fact, the crystal structure of *S. pneumoniae* α-enolase revealed that the two C-terminal lysine residues are significantly less exposed than the internal plasminogen-binding motif (34).

In this study, we constructed an *in silico* model of GAS SEN, based on the pneumococcal octameric α-enolase crystal structure, and validated this model using ion mobility (IM) mass spectrometry (MS). Site-directed mutagenesis followed by structural and functional analyses revealed that Lys^{344} plays a crucial role in structural integrity and enzymatic function. Furthermore, we demonstrate that the plasminogen-binding motif residues Lys^{252} and Lys^{255} and the C-terminal Lys^{434} and Lys^{435} residues are located adjacently in the GAS SEN structure and play a concerted role in the binding of human plasminogen.

EXPERIMENTAL PROCEDURES

Site-directed Mutagenesis—The pET14bSEN expression vector encoding an N-terminal His_6-tagged SEN cloned from the M6 GAS strain D471 (32) was used to construct site-directed mutants. Mutants $SEN^{K435L}$and $SEN^{\Delta 434-435}$ were as described previously (32). Lysine residues of interest within SEN were substituted with either alanine or glutamic acid by QuikChange® XL site-directed mutagenesis (Stratagene), using primers listed in supplemental Table S1 and methods previously described (8). DNA sequence analysis was used to confirm introduced mutations using primers given in supplemental Table S1, and sequence reactions were performed using Terminator-ready reaction mix (Applied Biosystems) and methods described elsewhere (8). Samples were electrophoresed using an Applied Biosystems 3130*xl* genetic analyzer (Applied Biosystems), and sequence data were analyzed using Applied Biosystems DNA sequencing analysis software v 5.2 (Applied Biosystems).

Protein Expression and Purification—pET14bSEN and SEN mutant constructs were transformed into competent *Escherichia coli* BL21 STAR (DE3) cells and grown in LB medium supplemented with 100 μg ml^{-1} ampicillin at 37 °C to an absorbance at 600 nm of 0.6. Expression was conducted as described previously (35). The pure proteins were dialyzed into phosphate-buffered saline, and protein concentration was determined using a bicinchoninic acid protein assay kit (Sigma-Aldrich).

Nanoelectrospray-Ionization Mass Spectrometry (ESI-MS)—Mass spectra were acquired on a Waters Q-ToF Ultima mass spectrometer, which had been modified for high mass operation (36) using a nanoESI source. 2 μl of a solution of each protein in 200 mM NH_4OAc (concentrations ranged from 3 to 8 μM, as monomer) were electrosprayed from gold-coated glass capillaries prepared in-house. Q-ToF instrument conditions included a capillary potential of 1.5 kV; cone, 140 V; radio frequency lens 1, 80 V; collision cell, 4 V; transport and aperture, 5 V, and the microchannel plate detector was set to 1,750 V. Collision cell gas pressure was adjusted to 3×10^{-2} mbar to provide sufficient collisional cooling to preserve non-covalent interactions and maintain the proteins in their native conformation. All spectra were externally calibrated using a cesium iodide spectrum and reference file and processed using MassLynx™ software.

Ion Mobility-Mass Spectrometry (IM-MS)—Ion mobility-mass spectrometry was performed on a Synapt HDMS™ system (Waters) (37), fitted with a 32,000 *m*/*z* quadrupole. Nanoelectrospray spectra were acquired using previously described protocols (38). The following voltages were used: capillary, 1.65 kV; sample cone, 40 V, "trap collision energy," 10 V; "transfer collision energy," 10 V; and a 0–30-V wave-height ramp in the drift cell. The gases used were nitrogen and argon in the T-Wave IM separator and collision cells, respectively. The pressures in the various stages were the following: backing, 4.5 mbar; trap, 6.2×10^{-2} mbar; IM, 0.44 mbar; and ToF, 1.6×10^{-6} mbar. Data were processed using MassLynx software, and the MS dimension was calibrated externally. All spectra are shown here with minimal smoothing, linear intensity scales, and no background subtraction. The collision cross-section for wild-type protein was measured using a previously described approach (39).

In Silico Modeling—Sequence searches using BLAST (40) identified α-enolase from *S. pneumoniae* as the protein with a known three-dimensional structure most closely related to GAS SEN (93% identity at the amino acid level). The octameric biological unit of *S. pneumoniae* α-enolase was constructed using crystal symmetry operators with the program PyMOL (DeLano Scientific LLC). This octameric structure was then used to model the structure of GAS SEN with the program Modeler (41). The model with the best Modeler objective function was selected. The model presented comprises eight copies

FIGURE 1. **Structural and biochemical analysis, molecular modeling, and plasminogen binding ability of recombinant wild-type SEN.** *A*, ribbon diagram of the model of wild-type SEN octamer modeled from the crystal structure of octameric *S. pneumoniae* α-enolase. *B* and *C*, ESI-MS (*inset*: spectrum transformed to mass scale) (*B*) and IM-MS plots showing the octameric structure of recombinant wild-type SEN (*C*). *D*, far-UV circular dichroism spectrum demonstrating the predominantly α-helical secondary structure of recombinant wild-type SEN, as shown by the minima at 209 and 222 nm. *E*, enzymatic activity of recombinant wild-type SEN. The graph shown was constructed from the averages of three independent experiments, with *error bars* indicating the standard deviation. *deg*, degree. *F*, representative surface plasmon resonance sensorgram for recombinant wild-type SEN (100 nM, as monomer) binding to human Glu-plasminogen; 10,200 response units of ligand had been immobilized on a CM5 chip using amine-coupling chemistry.

of GAS SEN residues 1–435. Theoretical collision cross-sections were calculated as described previously (38) using the projection approximation of Mobcal software (42).

Far-UV Circular Dichroism (CD) Spectroscopy—CD spectra were obtained on a JASCO J-810 CD spectropolarimeter at room temperature as described previously (43). Deconvolution of the spectra to estimate secondary structure was achieved using the CDSSTR program (44) in the DICHROWEB Online Circular Dichroism Analysis suite (45). Data from the 240–190-nm region with a data interval of 1 nm were used with Reference Set 4 optimized for this region.

Enzymatic (α-Enolase) Activity—The catalytic activity of the SEN mutants was compared with the wild-type protein by measuring the conversion of 2-phosphoglycerate to phosphoenolpyruvate. The reaction was performed essentially as described previously (32).

Purification of Human Glu-Plasminogen—The circulating form of human plasminogen (Glu-plasminogen) was purified from human plasma using lysine-Sepharose 4B affinity chromatography as described previously (46). Glu-plasminogen was dialyzed into phosphate-buffered saline, and protein concentration was determined using a bicinchoninic acid protein assay kit (Sigma-Aldrich).

Surface Plasmon Resonance of Plasminogen Binding—The binding of recombinant wild-type and mutant SEN proteins to Glu-plasminogen was measured using a BIAcore T100 optical biosensor (GE Healthcare). Glu-plasminogen (14.93 μM in 10 mM sodium acetate buffer, pH 4.0) was coupled at 10 μl min^{-1} (7 min) onto *N*-hydroxysuccinimide/*N*-ethyl-*N*′-(3-diethylaminopropyl) carbodiimide-activated CM5 sensor chips to yield 10,200 response units of bound protein. Binding of SEN proteins was done at 25 °C in 10 mM HEPES, pH 7.4, 0.15 M NaCl, 3 mM EDTA, 0.05% surfactant P20, using a flow rate of 30 μl min^{-1}. Association and disso-

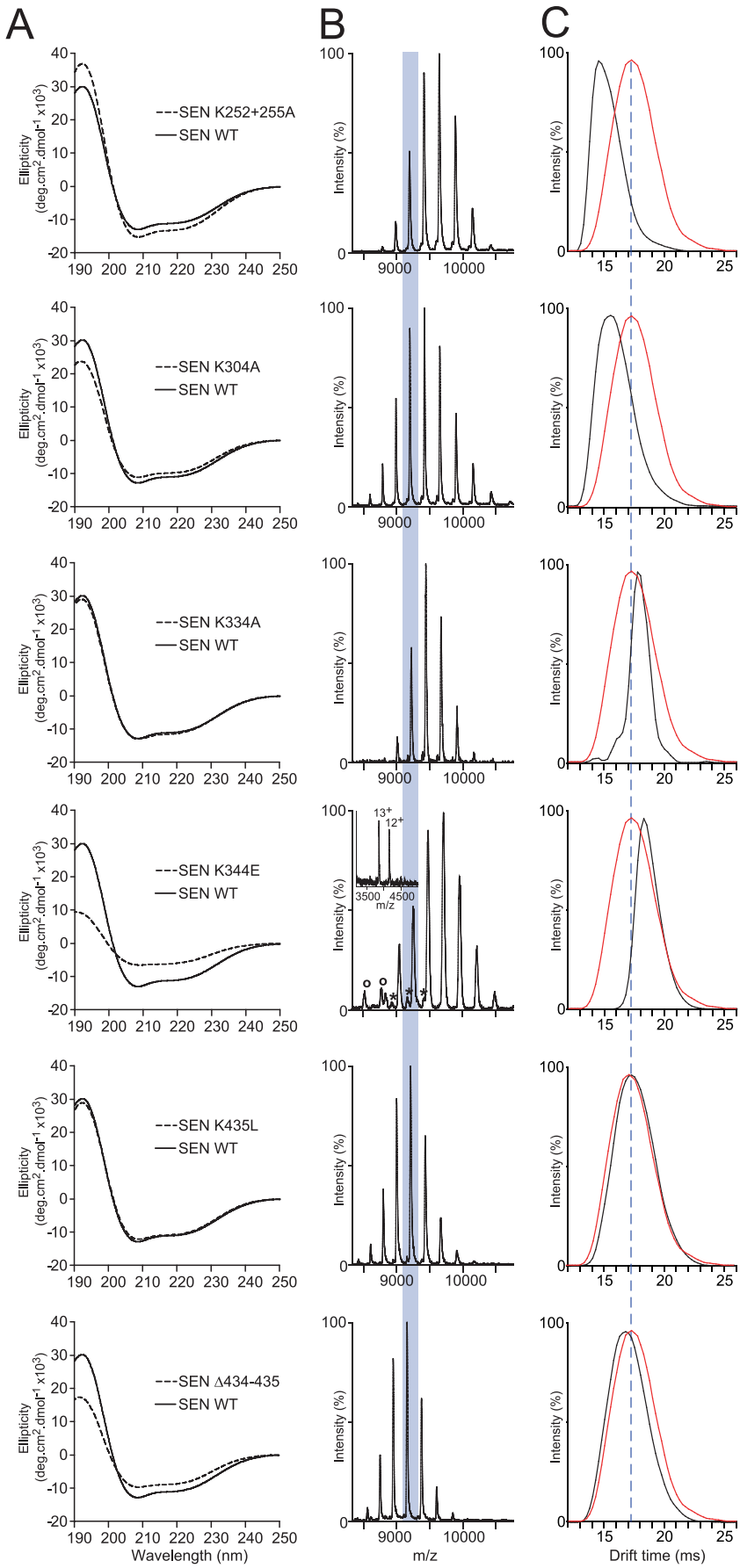

ciation times were 500 and 600 s, respectively. Affinity surfaces were regenerated between SEN injections with 10 mM glycine·HCl, pH 1.5 (60 s at 10 μl min^{-1}) followed by 4 M $MgCl_2$ (60 s at 5 μl min^{-1}). Kinetic models could not suitably fit the data using the Biacore T100 evaluation software, likely due to the large molecular size of the SEN analytes and consequent mass transfer rate limitations, so the relative abilities of SEN variants to bind plasminogen were assessed qualitatively. Binding was assayed in quadruplicate, through two different flow cells and on two independently prepared sensor chips; relative binding responses for mutant and wild-type SENs were consistently observed.

Ligand Blot of Plasminogen Binding—Ligand blot analysis of recombinant SEN proteins incubated with human Glu-plasminogen (5 μg ml^{-1}) was performed as described previously (46). Rabbit anti-human plasminogen diluted 1:500 and goat anti-rabbit IgG horseradish peroxidase conjugate (Bio-Rad) diluted 1:1000 were used as primary and secondary antibodies, respectively.

RESULTS

Characterization of Wild-type GAS SEN—The structure of wild-type SEN was examined by means of *in silico* modeling, MS, and far-UV CD spectroscopy. We first constructed an *in silico* model of octameric GAS SEN (Fig. 1*A*) based on the known crystal structure of *S. pneumoniae* α-enolase (34). The theoretical collision cross-section for this homology-modeled octamer was calculated to be 12,100 Å^2. This was achieved by using Mobcal software (42), modified for modeling large protein assemblies (38). Briefly, this approach uses the atomic structure without coarse graining and assumes free tumbling of the protein in the gas phase, thereby resulting in a rotationally averaged collision cross-section. To characterize GAS α-enolase, we expressed and purified the wild-type protein utilizing a His_6 tag at the N terminus. MS of SEN under conditions where preservation of the native state non-covalent assembly is favored (48) (Fig. 1*B*) exhibited a series of peaks in the range 8,600–10,200 *m*/*z*, corresponding to 46$^+$ through 39$^+$ charge states of SEN. Transformation to a mass scale (Fig. 1*B*, *inset*) gave an estimated mass of 395.9 kDa, corresponding well with the predicted mass of the octamer (394.9 kDa).

IM-MS Analysis of Wild-type GAS SEN—IM-MS data for wild-type SEN were acquired using traveling wave-based separation and revealed drift times for the three major ions of 14.8 (44$^+$), 15.7 (43$^+$), and 16.9 ms (42$^+$) (Fig. 1*C*). Determining collision cross-sections for such traveling wave IM-MS data is not currently possible without calibration; therefore, we employed an alternative strategy based on measuring the minimum wave height at which ions are pushed the length of the cell by the first wave (39). From this direct measurement of collision cross-section, we obtained a value of 12,800 ± 580 Å^2 for octameric wild-type SEN (mean of the four principal charge states, ±two standard deviations). A CD spectrum of wild-type SEN showed minima at 222 and 209 nm, indicating a primarily α-helical secondary structure (Fig. 1*D*). Deconvolution of the CD spectrum suggested that the structure contains ~48% α-helix, which correlates well with the 42% helical content of the *in silico* model (Fig. 1*A*).

Functional Analysis of Wild-type GAS SEN—We next undertook functional analysis of purified SEN to determine the enzymatic activity and ability to bind human plasminogen. The α-enolase activity of SEN (conversion of 2-phosphoglycerate to phosphoenolpyruvate) was measured spectrophotometrically at 240 nm. The initial rate of phosphoenolpyruvate formation for wild-type SEN was 0.123 μmol min^{-1} μg^{-1} of recombinant protein (Fig. 1*E*). Surface plasmon resonance was used to demonstrate the plasminogen binding ability of SEN in a qualitative way. Human Glu-plasminogen was immobilized onto a CM5 sensor chip using amine-coupling chemistry, and 100 nM SEN (as monomer) was made to flow over the surface. As expected for such a large analyte molecule, SEN binding occurred at a slow rate that was limited by mass transfer and made to dissociate slowly (Fig. 1*F*).

Structural Analysis of SEN Mutants—Site-directed mutagenesis was undertaken to examine the role of selected lysine residues in the structural integrity and function of GAS SEN. Lysine residues for analysis were chosen based on their known role in plasminogen binding by GAS SEN (SEN^{K435L} and $SEN^{\Delta 434-435}$) (32) or *S. pneumoniae* α-enolase ($SEN^{K252+255A}$) (33), on their implication in α-enolase secretion (SEN^{K344E}) (49), or on being otherwise located in the C-terminal domain of the GAS SEN monomer (SEN^{K304A} and SEN^{K334A}). Each of these lysine residues was predicted to be surface-exposed in the structural model of the GAS SEN monomer (supplemental Fig. S1). All of the purified mutant proteins except for SEN^{K344E} were found to retain the full α-helical content of the wild-type protein, as deduced from the intensities of minima at 222 and 209 nm in their CD spectra (Fig. 2*A*). ESI-MS spectra showed that aside from minor shifts in the charge state distributions due to the replacement or removal of lysine residues, all mutants retained the octameric structural characteristic of wild-type SEN (Fig. 2, *B* and *C*). SEN^{K344E} however, was clearly present in two additional multimeric forms, as evidenced by the peak series interspersed within those arising from the octamer, as well as a pair of charge states at considerably lower values of 3,800–4,200 *m*/*z*. A careful examination of these charge state series revealed that the SEN^{K344E} octamer was partially dissociated in solution into heptamers, hexamers, and monomers. Significantly, this appeared to be a solution-phase phenomenon rather than a product of dissociation in the gas phase as the narrow monomer charge state distribution is characteristic of a folded protein (50), and gas-phase dissociation occurs via monomer unfolding (51). Thus, introduction of an acidic residue at position 344 resulted in significant structural destabilization of SEN.

IM-MS Analysis of SEN Mutants—For each of the mutants and wild-type SEN, the drift times of the 43$^+$ charge states (Fig.

FIGURE 2. **Structural analysis of recombinant SEN mutants.** *A*, far-UV circular dichroism spectra comparing wild-type (*WT*) SEN (*solid lines*) and each of the mutant forms (*dashed lines*). *deg*, degree. *B*, ESI-mass spectra illustrating the major charge state series for each of the mutant octamers, with the 43$^+$ charge state highlighted. SEN^{K344E} was observed to contain minor amounts of heptamer (*) and monomer (*o*) (shown in *insets*). *C*, IM-mass spectra showing the drift time for the 43$^+$ charge state of each mutant (*black profiles*) when compared with that of wild-type SEN (*red profiles*).

2*B*, *shaded*) at the same acceleration voltage were extracted (Fig. 2*C*). The drift time of wild-type SEN is overlaid in *red* on the SEN mutant data in each panel so that differences are readily apparent. The mutations had the effect of shortening, lengthening, or not changing the octamer drift time relative to that of the wild-type protein. Structural integrity was maintained for all mutants except SEN^{K344E}, which exhibited a long drift time indicative of structural instability, consistent with its far-UV CD spectrum (Fig. 2*A*), and solution-phase dissociation into species smaller than the octamer (Fig. 2*B*). The remaining octameric species clearly have a greater collision cross-section, which is responsible for the augmented drift time. Of the other mutants, $SEN^{K252+255A}$ and SEN^{K304A} clearly assumed more compact quaternary states, whereas SEN^{K334A}, SEN^{K435L}, and $SEN^{\Delta 434-435}$ remained similar in molecular shape to the wild-type SEN. These differences can be reflective of either changes to the quaternary structure of the protein in solution or an alteration of the susceptibility to structural changes that occur as a result of gas-phase activation (52).

Functional Analysis of SEN Mutants—Determination of α-enolase enzymatic activity and plasminogen binding ability by ligand blotting and surface plasmon resonance was used for functional comparison of SEN mutants with the wild-type protein. Enzymatic activity was retained for $SEN^{K252+255A}$ (0.091 μmol min^{-1} μg^{-1}), SEN^{K304A} (0.095 μmol min^{-1} μg^{-1}), and SEN^{K435L} (0.069 μmol min^{-1} μg^{-1}), was reduced in SEN^{K334A} (0.026 μmol min^{-1} μg^{-1}) and $SEN^{\Delta 434-435}$ (0.015 μmol min^{-1} μg^{-1}), and was completely abolished in SEN^{K344E} (<0.004 μmol min^{-1} μg^{-1}) (supplemental Fig. S2). Ligand blotting using denatured wild-type and mutant forms of SEN with human Glu-plasminogen showed that all mutants bound plasminogen except for SEN^{K435L}

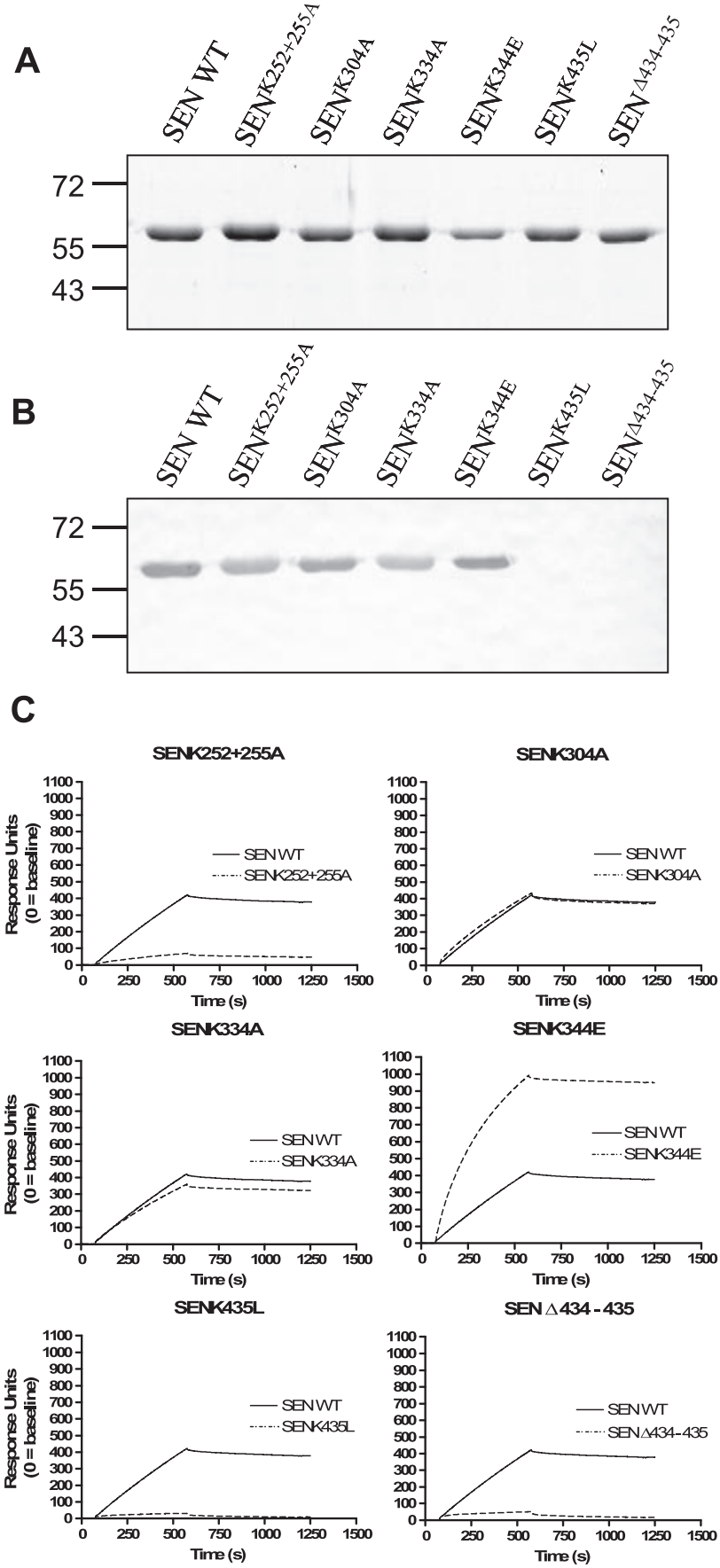

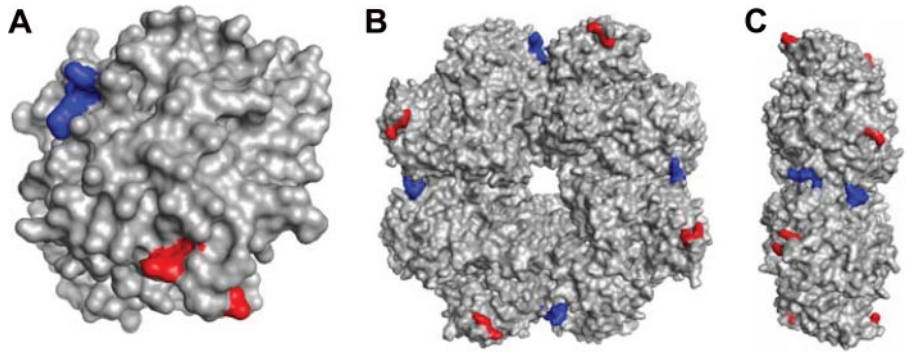

FIGURE 4. **Homology model of SEN based on the crystal structure of *S. pneumoniae* α-enolase showing lysine residues implicated in plasminogen binding.** *A*, monomeric subunit. *B*, octameric structure. *C*, side view of octameric structure. Internal lysine residues at positions 252 and 255 are colored *red*, and C-terminal lysines are colored *blue*.

and $SEN^{\Delta 434-435}$ (Fig. 3, *A* and *B*). When the plasminogen binding ability of the SEN mutants in native conformation was examined using surface plasmon resonance, SEN^{K304A} and SEN^{K334A} bound Glu-plasminogen equivalently to wild type, whereas SEN^{K344E} displayed apparently increased plasminogen binding ability. This increase is probably due to the presence of lower oligomeric forms, whose binding would suffer less from mass transfer limitations, and indeed, the shape of the binding curve also supports this interpretation. The ability to bind human Glu-plasminogen was greatly diminished for $SEN^{K252+255A}$, SEN^{K435L}, and $SEN^{\Delta 434-435}$ (Fig. 3*C*). These data thus suggest strongly that plasminogen interacts with both lysine pairs (252 + 255 and 434 + 435) in GAS SEN.

Modeling Data—The crystal structure of *S. pneumoniae* α-enolase, determined at 2 Å resolution, revealed an octameric structure (34). In the GAS SEN model, lysines 252 and 255 are located in a surface-exposed loop at the edge of the toroidal octameric protein (Fig. 4). Lysines 434 and 435 are similarly located on the surface of the protein, near a dimer interface in the octamer. Because of their surface location, mutations of these lysines would not be expected to have any gross structural effects, consistent with our CD and MS data. Lysines 304 and 334 are also exposed on the surface, on a straight line between the Lys^{252}–Lys^{255} and Lys^{434}–Lys^{435} pairs (supplemental Fig. S1). By contrast, lysine 344 is in a different region of the protein (supplemental Fig. S1), partially buried at the active site at the center of the monomer adjacent to the Mg^{2+}-binding site, consistent with the effect of the SEN^{K344E} mutation on structure and enzymatic activity (49).

DISCUSSION

Few techniques are available for the structural analysis of complex protein macromolecules. Nonetheless, stunning advances have been made through acquisition of the three-dimensional structures of protein complexes using x-ray crystallography; examples include photosystems I (53) and II (54) and the bacterial ribosome (55). However, significant impediments to the acquisition of structural data for biological macromolecules include the purification of sufficient amounts of the protein complex and the formation of the necessary well diffracting protein crystals (56, 57). In the absence of x-ray crystallography data, *in silico* protein modeling can be undertaken, utilizing known structural information of related protein homologs as scaffolds (58). The validation of *in silico*-generated protein structures creates a paradox often only resolved by x-ray crystallographic analysis.

In recent years, the technique of MS has evolved into a powerful tool for the interrogation of native oligomeric protein structure, in particular the stoichiometry of protein assemblies and the spatial distribution of subunits therein (59, 60). A further exciting addition to the field of MS is the coupling of ion mobility separation to mass analysis, which provides insights into the shape of intact protein complexes based on their drift time in a mobility cell (38). Studies have revealed that the charge state of a protein is highly dependent upon its quaternary structure and that information about the physical size of proteins and their complexes can be derived from drift times (61).

In the present work, we applied CD spectroscopy, ESI-MS, and IM-MS to the structural characterization of wild-type SEN and six mutant forms. Such an approach affords a rapid estimate of quaternary size and gross structural shape using only femtomolar quantities of protein, obviating the need for protein crystallization. Based on mass, it was found that, except for SEN^{K344E}, all SEN variants existed exclusively as octamers. The SEN^{K344E} mutant was clearly destabilized, giving rise to a mixture of octamers, heptamers, hexamers, and monomers. Furthermore, the apparent reduction in α-helical content as observed by far-UV CD is consistent with a loosening of the overall macromolecular shape of this mutant and could account for the observed IM drift time, which was greater than wild-type SEN and each of the other mutants. These structural changes in the SEN^{K344E} mutant may also result in improved access between the lysine-binding kringle domains of plasminogen and SEN, accounting for the improved plasminogen binding capacity for this SEN mutant.

The ability of SEN to bind plasminogen has been demonstrated for GAS and other bacterial species (27, 33). Although the plasminogen binding ability of GAS SEN has been linked to the C-terminal lysine residues (434 + 435), here we show that internal lysine residues (252 + 255) also contribute to plasmin-

FIGURE 3. **Plasminogen binding ability of SEN mutants.** *A*, Coomassie Brilliant Blue-stained 12% SDS-PAGE reducing gel of SEN wild type (*WT*) and mutants. *B*, corresponding ligand blot. Proteins were transferred to a membrane, incubated with Glu-plasminogen, and probed with antiserum specific for human plasminogen. *C*, surface plasmon resonance sensorgrams for recombinant wild-type and mutant SEN proteins binding at 100 nM (as monomer) to immobilized human Glu-plasminogen (10,200 response units).

ogen binding, as described for the closely related *S. pneumoniae* α-enolase (32, 33). When examining the model of octameric SEN validated in this study, the C-terminal lysine residues (434 + 435) are found in proximity to the internal lysine residues (252 + 255). The distance separating adjacent plasminogen-binding lysine pairs of 30 Å approximates the distance between the binding sites in the kringle domains (K1–K3) of plasminogen (47, 62). These observations suggest that these two binding sites play a crucial and concerted role in plasminogen binding. IM-MS provides a powerful new tool for protein structure/function analysis.

Acknowledgments—We thank Prof. Judith Kornblatt (Concordia University) for providing the 2-phosphoglycerate substrate for enolase enzymatic assays, and Tara Pukala, Brandon Ruotolo (both University of Cambridge), and Kevin Giles (Waters UK) for cross-section measurements of wild-type SEN.

REFERENCES

1. Carapetis, J. R., Steer, A. C., Mulholland, E. K., and Weber, M. (2005) *Lancet Infect. Dis.* **5,** 685–694
2. Cunningham, M. W. (2000) *Clin. Microbiol. Rev.* **13,** 470–511
3. Tart, A. H., Walker, M. J., and Musser, J. M. (2007) *Trends Microbiol.* **15,** 318–325
4. Carapetis, J. R., Walker, A. M., Hibble, M., Sriprakash, K. S., and Currie, B. J. (1999) *Epidemiol. Infect.* **122,** 59–65
5. McArthur, J. D., McKay, F. C., Ramachandran, V., Shyam, P., Cork, A. J., Sanderson-Smith, M. L., Cole, J. N., Ringdahl, U., Sjöbring, U., Ranson, M., and Walker, M. J. (2008) *FASEB J.* **22,** 3146–3153
6. Walker, M. J., McArthur, J. D., McKay, F., and Ranson, M. (2005) *Trends Microbiol.* **13,** 308–313
7. Sanderson-Smith, M. L., Walker, M. J., and Ranson, M. (2006) *J. Biol. Chem.* **281,** 25965–25971
8. Sanderson-Smith, M. L., Dowton, M., Ranson, M., and Walker, M. J. (2007) *J. Bacteriol.* **189,** 1435–1440
9. Pancholi, V., and Fischetti, V. A. (1992) *J. Exp. Med.* **176,** 415–426
10. Pancholi, V., and Chhatwal, G. S. (2003) *Int. J. Med. Microbiol.* **293,** 391–401
11. Kuusela, P., Ullberg, M., Saksela, O., and Kronvall, G. (1992) *Infect. Immun.* **60,** 196–201
12. Winram, S. B., and Lottenberg, R. (1998) *Microbiology* **144,** 2025–2035
13. D'Costa, S. S., and Boyle, M. D. P. (1998) *Microb. Pathog.* **24,** 341–349
14. Wang, H., Lottenberg, R., and Boyle, M. D. P. (1995) *J. Infect. Dis.* **171,** 85–92
15. McKay, F. C., McArthur, J. D., Sanderson-Smith, M. L., Gardam, S., Currie, B. J., Sriprakash, K. S., Fagan, P. K., Towers, R. J., Batzloff, M. R., Chhatwal, G. S., Ranson, M., and Walker, M. J. (2004) *Infect. Immun.* **72,** 364–370
16. Kapur, V., Kanjilal, S., Hamrick, M. R., Li, L. L., Whittam, T. S., Sawyer, S. A., and Musser, J. M. (1995) *Mol. Microbiol.* **16,** 509–519
17. Walker, M. J., Hollands, A., Sanderson-Smith, M. L., Cole, J. N., Kirk, J. K., Henningham, A., McArthur, J. D., Dinkla, K., Aziz, R. K., Kansal, R. G., Simpson, A. J., Buchanan, J. T., Chhatwal, G. S., Kotb, M., and Nizet, V. (2007) *Nat. Med.* **13,** 981–985
18. Sun, H., Ringdahl, U., Homeister, J. W., Fay, W. P., Engleberg, N. C., Yang, A. Y., Rozek, L. S., Wang, X., Sjöbring, U., and Ginsburg, D. (2004) *Science* **305,** 1283–1286
19. Sanderson-Smith, M. L., Dinkla, K., Cole, J. N., Cork, A. J., Maamary, P. G., McArthur, J. D., Chhatwal, G. S., and Walker, M. J. (2008) *FASEB J.* **22,** 2715–2722
20. Parry, M. A., Zhang, X. C., and Bode, I. (2000) *Trends Biochem. Sci.* **25,** 53–59
21. Saksela, O., and Rifkin, D. B. (1988) *Annu. Rev. Cell Biol.* **4,** 93–126
22. Danø, K., Andreasen, P. A., Grøndahl-Hansen, J., Kristensen, P., Nielsen, L. S., and Skriver, L. (1985) *Adv. Cancer Res.* **44,** 139–266
23. Ponting, C. P., Marshall, J. M., and Cederholm-Williams, S. A. (1992) *Blood Coagul. Fibrinolysis* **3,** 605–614
24. Reddy, K. N., and Markus, G. (1972) *J. Biol. Chem.* **247,** 1683–1691
25. Berge, A., and Sjöbring, U. (1993) *J. Biol. Chem.* **268,** 25417–25424
26. Lottenberg, R., Broder, C. C., Boyle, M. D., Kain, S. J., Schroeder, B. L., and Curtiss, R., 3rd (1992) *J. Bacteriol.* **174,** 5204–5210
27. Pancholi, V., and Fischetti, V. A. (1998) *J. Biol. Chem.* **273,** 14503–14515
28. Pancholi, V. (2001) *Cell. Mol. Life Sci.* **58,** 902–920
29. Wold, F. (1971) in *The Enzymes* (Boyer, P. D., ed) Vol. 5, 3rd Ed., pp. 499–538, Academic Press, New York
30. Cole, J. N., Ramirez, R. D., Currie, B. J., Cordwell, S. J., Djordjevic, S. P., and Walker, M. J. (2005) *Infect. Immun.* **73,** 3137–3146
31. Bergmann, S., and Hammerschmidt, S. (2007) *Thromb. Haemost.* **98,** 512–520
32. Derbise, A., Song, Y. P., Parikh, S., Fischetti, V. A., and Pancholi, V. (2004) *Infect. Immun.* **72,** 94–105
33. Bergmann, S., Wild, D., Diekmann, O., Frank, R., Bracht, D., Chhatwal, G. S., and Hammerschmidt, S. (2003) *Mol. Microbiol.* **49,** 411–423
34. Ehinger, S., Schubert, W. D., Bergmann, S., Hammerschmidt, S., and Heinz, D. W. (2004) *J. Mol. Biol.* **343,** 997–1005
35. Cole, J. N., Sanderson-Smith, M. L., Cork, A. J., Henningham, A., Conlan, F., Ranson, M., McArthur, J. D., and Walker, M. J. (2006) in *Molecular Biology of Streptococci* (Hakenbeck, R., and Chhatwal, G. S., eds), pp. 359–379, Scientific Press, Hethersett, UK
36. Benesch, J. L., Ruotolo, B. T., Sobott, F., Wildgoose, J., Gilbert, A., Bateman, R., and Robinson, C. V. (2009) *Anal. Chem.* **81,** 1270–1274
37. Pringle, S. D., Giles, K., Wildgoose, J. L., Williams, J. P., Slade, S. E., Thalassinos, K., Bateman, R. H., Bowers, M. T., and Scrivens, J. H. (2007) *Int. J. Mass Spectrom.* **261,** 1–12
38. Ruotolo, B. T., Benesch, J. L., Sandercock, A. M., Hyung, S. J., and Robinson, C. V. (2008) *Nat. Protoc.* **3,** 1139–1152
39. Giles, K., Wildgoose, J., and Langridge, D. (2008) in *56th ASMS Conference on Mass Spectrometry*, Denver, Colorado, June 1–5, 2008, American Society for Mass Spectrometry, Santa Fe, NM
40. Johnson, M., Zaretskaya, I., Raytselis, Y., Merezhuk, Y., McGinnis, S., and Madden, T. L. (2008) *Nucleic Acids Res.* **36,** W5–9
41. Eswar, N., Webb, B., Marti-Renom, M. A., Madhusudhan, M. S., Eramian, D., Shen, M. Y., Pieper, U., and Sali, A. (2007) *Curr. Protoc. Protein Sci.* **2,** Unit 2.9
42. Mesleh, M. F., Hunter, J. M., Shvartsburg, A. A., Schatz, G. C., and Jarrold, M. F. (1996) *J. Phys. Chem.* **100,** 16082–16086
43. Morris, A. M., Treweek, T. M., Aquilina, J. A., Carver, J. A., and Walker, M. J. (2008) *FEBS J.* **275,** 5885–5898
44. Sreerama, N., and Woody, R. W. (2000) *Anal. Biochem.* **287,** 252–260
45. Lobley, A., Whitmore, L., and Wallace, B. A. (2002) *Bioinformatics* **18,** 211–212
46. Sanderson-Smith, M., Batzloff, M., Sriprakash, K. S., Dowton, M., Ranson, M., and Walker, M. J. (2006) *J. Biol. Chem.* **281,** 3217–3226
47. Geiger, J. H., and Cnudde, S. E. (2004) *J. Thromb. Haemost.* **2,** 23–34
48. Benesch, J. L., and Robinson, C. V. (2006) *Curr. Opin. Struct. Biol.* **16,** 245–251
49. Boël, G., Pichereau, V., Mijakovic, I., Mazé, A., Poncet, S., Gillet, S., Giard, J. C., Hartke, A., Auffray, Y., and Deutscher, J. (2004) *J. Mol. Biol.* **337,** 485–496
50. Benesch, J. L., Sobott, F., and Robinson, C. V. (2003) *Anal. Chem.* **75,** 2208–2214
51. Benesch, J. L., Aquilina, J. A., Ruotolo, B. T., Sobott, F., and Robinson, C. V. (2006) *Chem. Biol.* **13,** 597–605
52. Benesch, J. L. P. (2009) *J. Am. Soc. Mass Spectrom.* **20,** 341–348
53. Jordan, P., Fromme, P., Witt, H. T., Klukas, O., Saenger, W., and Krauss, N. (2001) *Nature* **411,** 909–917
54. Zouni, A., Witt, H. T., Kern, J., Fromme, P., Krauss, N., Saenger, W., and Orth, P. (2001) *Nature* **409,** 739–743
55. Schuwirth, B. S., Borovinskaya, M. A., Hau, C. W., Zhang, W., Vila-Sanjurjo, A., Holton, J. M., and Cate, J. H. (2005) *Science* **310,** 827–834
56. Byrne, B., and Iwata, S. (2002) *Curr. Opin. Struct. Biol.* **12,** 239–243
57. Riekel, C., Burghammer, M., and Schertler, G. (2005) *Curr. Opin. Struct.*

Biol. **15,** 556–562
58. Eswar, N., John, B., Mirkovic, N., Fiser, A., Ilyin, V. A., Pieper, U., Stuart, A. C., Marti-Renom, M. A., Madhusudhan, M. S., Yerkovich, B., and Sali, A. (2003) *Nucleic Acids Res.* **31,** 3375–3380
59. Benesch, J. L., Ruotolo, B. T., Simmons, D. A., and Robinson, C. V. (2007) *Chem. Rev.* **107,** 3544–3567
60. Hernández, H., Dziembowski, A., Taverner, T., Séraphin, B., and Robinson, C. V. (2006) *EMBO Rep.* **7,** 605–610
61. Ruotolo, B. T., Giles, K., Campuzano, I., Sandercock, A. M., Bateman, R. H., and Robinson, C. V. (2005) *Science* **310,** 1658–1661
62. Abad, M. C., Arni, R. K., Grella, D. K., Castellino, F. J., Tulinsky, A., and Geiger, J. H. (2002) *J. Mol. Biol.* **318,** 1009–1017